ELSEVIER

Journal of Fluids and Structures 20 (2005) 35–49

JOURNAL OF FLUIDS AND STRUCTURES

www.elsevier.com/locate/jfs

Application of an improved cell mapping method to bilinear stiffness aeroelastic systems

Q. Ding[a,*], J.E. Cooper[b], A.Y.T. Leung[c]

[a]*Department of Mechanics, Tianjin University, Tianjin 300072, P.R. China*
[b]*School of Engineering, University of Manchester, Manchester M13 9PL, UK*
[c]*Department of Building and Construction, City University of Hong Kong, Tatchee Avenue, HKSAR, China*

Received 1 February 2001; accepted 16 September 2004
Available online 2 January 2005

Abstract

A "mapping trajectory pursuit (MTP)" is introduced to improve the cell mapping techniques based on spatial Poincaré sections. Such an improvement enables the cell mapping method to determine the exact properties of all cells with less computer memory and computational time. For the purpose of prediction of the stability boundary as a function of initial conditions (domains of attraction), an initial condition region is defined besides the domain of interest. The proposed CM method is used to analyse the aeroelastic behaviour of an aeroelastic system with bilinear structural nonlinearity. Different types of motions including damped stable motion, limit cycle oscillation, complicated periodic motion, chaotic motion and divergent flutter are determined as a function of initial conditions (domains of attraction). The results compare well with that from stability analysis of the system. The bifurcation diagrams are also obtained using the method to reveal the influence of disturbances on the dynamical behaviour of the system over a broad range of air speed.

1. Introduction

A nonlinear dynamical system can have several qualitatively distinct steady state solutions depending on the initial conditions. A global behaviour analysis of such systems by direct numerical integration is often extremely time-consuming and error prone. For this reason, a "simple cell mapping" (SCM) method was proposed by Hsu (1980) and Hsu and Guttalu (1980). The method is based on the discretization of the state space of a dynamical system into small regions called cells, and the subsequent construction of an integer-type mapping of these cells. Many computational techniques based on the concept of cell mapping have also been developed, e.g. "generalized cell mapping" (GCM) by Hsu (1981, 1982, 1987) and "interpolated cell mapping" (ICM) by Tongue and Gu (1988).

Despite their advantages in comparison with direct integration, these methods are quite computer time and computer memory consuming, when applied to high-order dynamical systems. A further development to reduce the amount of cells used in the calculation led to the introduction of "Poincaré-like simple cell mapping" (PLSCM) by Levitas et al. (1994) and "Poincaré linear interpolated cell mapping" (PLICM) by Levitas and Weller (1995), which combine the use of spatial Poincaré sections with SCM and ICM, respectively. The introduction of Poincaré sections allows considerable

*Corresponding author. Tel.: +86 22 2740 8667.
E-mail address: qding@public.tpt.tj.cn (Q. Ding).

0889-9746/$ - see front matter
doi:10.1016/j.jfluidstructs.2004.09.003

reductions in the number of cells involved and therefore appears to be appropriate for the study of the multi-degree-of-freedom dynamical systems. However, the solutions of the system are approximate due to the error incurred at the beginning of every iteration. Either the values at the mid-points of cells or at the interpolated points of the cell vertices are used as the initial values of the successive integrations rather than at the actual mapped position. Thus the limitation of the small cell size to minimize the numerical error prevents the application of the methods to high-dimensional systems. For interpolated-type methods, the cells generated may wrongly be determined as "sink cells" even if the trajectory leaves the domain of interest only temporarily and will return back later during iterations.

Recently, many investigations have been made for structurally nonlinear aeroelastic systems. Lumped nonlinear parameters including freeplay, bilinear and cubic stiffness, have been known to have significant effects on the aeroelastic responses of aerosurfaces (Kim and Lee, 1996; Librescu and Chiocchia, 2003; Price et al., 1994; Singh and Brenner, 2003; Tang et al., 1998; Yang and Zhao, 1990; Zhao and Yang, 1990). Depending on the degree of nonlinearity, the behaviour of the airfoil was shown to be strongly dependent on the initial conditions. In fact, the influence of the initial conditions on the behaviour of airfoils is one of the main tasks of aeroelastic analysis. The results are referred to as the stability boundary in terms of the initial conditions (Price et al., 1994), boundary for different types of motion (Yang and Zhao, 1990), domains of attraction (Levitas et al., 1994; Levitas and Weller, 1995), or simply as parameter maps (Kim and Lee, 1996). Because the cell mapping techniques appear appropriate for the prediction of the boundaries of different types of motion depending on initial conditions, they have been applied in many engineering problems, including the global analysis of bifurcations of the Duffing–van-der-Pol oscillators under both additive and multiplicative random excitations (He et al., 2004), the global analysis of climate predictability (Mu et al., 2004), the optimal control of autonomous dynamical systems (Zufiria and Martinez-Marin, 2003), nonlinear vibrations of a rotor system with bearing clearance (Karlberg and Aidanpaa, 2003), multiple steady state solutions of a nonlinear system with time-delay (Raghothama and Narayanan, 2002) and the global dynamics of a damped flexible connecting rod (Chen and Chian, 2001). Nevertheless, to the authors' knowledge, the use of these techniques in the aeroelastic analysis of airfoils has not been reported yet.

In the present paper, a process of "mapping trajectory pursuit" (MTP) is incorporated into the cell mapping techniques using spatial Poincaré sections. The initial condition region is defined for the purpose of constructing the domains of attraction. Finally, it is used to analyse the flutter of a binary aeroelastic system with bilinear structural nonlinearity in torsion producing the initial condition boundaries of different types of motion.

2. Improvement on the cell mapping method

Consider an N-dimensional dynamical system described by the first-order ordinary differential equations

$$\frac{\mathrm{d}\mathbf{x}}{\mathrm{d}t} = F(\mathbf{x}), \quad F : R^N \to R^N \tag{1}$$

or

$$\frac{\mathrm{d}\mathbf{x}}{\mathrm{d}t} = F(\mathbf{x}, t), \quad F : R^N \times R \to R^N, \quad F(\bullet, t) = F(\bullet, t + T), \tag{2}$$

where T is the period of the time-periodic system (2). In SCM and ICM, Eq. (1) or (2) is first transformed into point-to-point mapping by numerical integration over a time interval τ such that

$$\mathbf{x}(n+1) = P(\mathbf{x}(n)), \quad P : R^N \to R^N, \tag{3}$$

which means that $\mathbf{x}(n)$, a point in the state space, is mapped by P after a period of time into a point $\mathbf{x}(n+1)$. For system (2), mapping (3) is defined as time Poincaré mapping when $\tau = T$. Then, cells in the state space can be defined according to the procedure described in Hsu (1980), Hsu and Guttalu (1980) or Hsu (1987) on the basis of the mapping (3).

2.1. Concept and algorithm

Instead of time sections with interval τ, one can obtain the point-to-point mapping (3) on a spatial Poincaré section Σ, which is an $(N-1)$-dimensional hyperplane in the R^N state space for both the autonomous system (1) and nonautonomous system (2). The hyperplane is transversal to the trajectories of the system. In PLICM (Levitas and Weller, 1995), only autonomous systems were considered. Such a procedure results in $P : \Sigma \to \Sigma$, and reduces the dimension of the space under study by keeping one of the coordinates constant. That coordinate is referred to as the Poincaré coordinate. The cell mapping is then applied to the intersecting points obtained on Σ. Selecting x_N as the

Poincaré coordinate, the cell $\mathbf{z} = (Z_1, Z_2, \ldots, Z_{N-1})$ contains all points $\mathbf{x} = (x_1, x_2, \ldots, x_{N-1}) \in \Sigma$ which satisfy

$$\left(Z_i - \frac{1}{2}\right)h_i \leqslant x_i < \left(Z_i + \frac{1}{2}\right)h_i, \quad i = 1, 2, \ldots, N-1, \tag{4}$$

where h_i is the cell size in the x_i-direction. Z_i is an integer, constructed by

$$Z_i = \mathrm{Int}\left[\frac{1}{h_i}x_i + \frac{1}{2}\right]. \tag{5}$$

The main idea of the proposed approach is to integrate Eq. (1) or (2) numerically with initial conditions $\mathbf{x}^0$, taken from the initial condition region $\mathbf{Q}$ as explained later, to obtain $\mathbf{x}^1$ which is the first intersection point of the trajectory with Σ, then obtain $\mathbf{x}^2$ by taking $\mathbf{x}^1$ as the initial condition, and $\mathbf{x}^3$, $\mathbf{x}^4$, …, in the similar way. Cells $\mathbf{z}^1$, $\mathbf{z}^2$, … are constructed according to Eq. (5) simultaneously with respect to $\mathbf{x}^1$, $\mathbf{x}^2$, … . Different from the existing cell mapping methods in which a cell is represented either by its mid-point or by an interpolated point, we record $\mathbf{x}^j (j \geqslant 1)$ as the representative point of cell $\mathbf{z}^j$ and use it to determine the state of the trajectory. To record the coordinate values of $\mathbf{x}^j$, an $(N-1)$-dimensional array $\boldsymbol{R}(\mathbf{z})$ is introduced. In component form, $R_i(\mathbf{z}^j) = x_i^j, \quad i = 1, 2, \ldots, N-1$. Besides, the three numbers defined in SCM, the group number $Gr(\mathbf{z})$, periodicity number $P(\mathbf{z})$ and the steps number $S(\mathbf{z})$ are also used.

Similar to the other cell mapping methods (Hsu, 1980; Hsu and Guttalu, 1980), the domain of interest $\mathbf{S} \subset \Sigma$, inside which the dynamics of the system is investigated, is defined and divided into cells to construct the cell space as needed. To determine the stability boundary in terms of the initial conditions or domains of attraction, an initial condition region $\mathbf{Q}$ is defined to cover all initial conditions to be investigated. $\mathbf{Q}$ is a subspace of R^N from one to N-dimension, so it can be different from $\mathbf{S}$ both in size and/or in dimension. $\mathbf{Q}$ is also divided into a number of "cells" as needed. But the cell sizes and coordinate directions in $\mathbf{Q}$ can be different from those in $\mathbf{S}$. Taking $N = 3$, for example, as presented in Fig. 1, $\Sigma \subset R^2$ is defined by $x_2 = \xi_2$. The mid-point of a "cell" in $\mathbf{Q}$ is taken as the initial conditions $\mathbf{x}^0$. The integrating trajectory starting from $\mathbf{x}^0$ intersects one-sidedly with $\mathbf{S}$ at $\mathbf{x}^1$,$\mathbf{x}^2$,… successively, constituting the point-to-point maps. The construction of cells both in $\mathbf{S}$ and $\mathbf{Q}$ is not shown in Fig. 1.

To apply the proposed method in determining the domains of attraction, the initial values of integration are taken from the initial condition region $\mathbf{Q}$ according to a rule set at the beginning. After an initial condition is chosen, the cells are constructed together with the numerical mapping points in $\mathbf{S}$. The first processing sequence ends when the global properties of all cells are determined. The next sequence begins with the next set of initial condition. The application ends after all points (or cells) inside the initial condition region $\mathbf{Q}$ have been dealt with.

The four possibilities in the processing sequence $\mathbf{z}^j$ are considered below.

(i) The newly generated cell $\mathbf{z}^j$ is virgin. In this case, $\mathbf{x}^j$ is recorded as the representing point of $\mathbf{z}^j$ and as the initial condition for the continuing integration in the present sequence. In SCM, each cell is represented by its mid-point, which also serves as the initial condition for further numerical integration.

(ii) The newly generated cell $\mathbf{z}^j$ has appeared before in the present sequence. A new periodic motion is found in this sequence only when the distance between the newly obtained point $\mathbf{x}^j$ and the representing point of the cell $\mathbf{z}^j$, $\left\|R(\mathbf{z}^j) - \mathbf{x}^j\right\|$, is less then a given small value d_1. When this happens, the processing sequence is terminated and all cells in this sequence are assigned to the newly obtained periodic motion. Otherwise, $\mathbf{x}^j$ is taken as the representing point of the cell $\mathbf{z}^j$ and the procedure is continued.

(iii) The newly generated cell $\mathbf{z}^j$ has appeared in one of the previous processing sequences. The current processing sequence is attractive to a cell with known global properties only when $\left\|R(\mathbf{z}^j) - \mathbf{x}^j\right\|$ is less then a given small value d_2. In

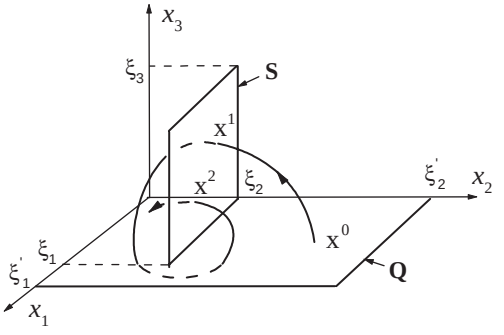

Fig. 1. An example of point-to-point maps for a three-dimensional system: $\mathbf{S} = \{(x_1, x_3) | 0 \leqslant x_1 \leqslant \xi_1,\ 0 \leqslant x_3 \leqslant \xi_3\} \subset \Sigma = \{x_2 = \xi_2\}$, $\mathbf{Q} = \{(x_1, x_2) | 0 \leqslant x_1 \leqslant \xi_1',\ 0 \leqslant x_2 \leqslant \xi_2'\}$.

such case, the processing sequence is terminated and the property of each cell in this sequence is the same as that of $\mathbf{z}^j$. Otherwise, the procedure is continued but $R(\mathbf{z}^j)$ is kept unchanged.

(iv) A cell is mapped outside $\mathbf{S}$. We do not construct cell for $\bar{\mathbf{x}}^j$ outside $\mathbf{S}$ but continue the numerical integration. The mapped points can either return into $\mathbf{S}$ again or leave farther and farther away from $\mathbf{S}$ implying divergence. In the former case, the mapped points inside $\mathbf{S}$ are dealt with continually in the same ways as in (i), (ii) or (iii). In the latter case, the processing sequence is terminated and all cells in this sequence inside $\mathbf{S}$ are assigned as "sink cells".

2.2. Some details of the algorithm

In carrying out the proposed approach, the following measures are used.

(i) As already mentioned, point-to-point mappings are performed by intersections of the trajectory of the system evolution with the hyperplane Σ. The intersection occurs if two successive output points from the integration in the Poincaré direction lie on the opposite sides of Σ at time t_i and t_{i+1}. Then the intersecting point $\bar{\mathbf{x}}^j$ is achieved by returning to the point $\mathbf{x}(t_i)$ and by integrating over a fine time step $\Delta\tau$. Generally, to ensure the repetitive intersections in the transient and steady state evolution trajectories, section Σ should be located at a zero value of velocity coordinate if the system has stable equilibrium points or stable limit cycles (Levitas and Weller, 1995). Taking $\Sigma = \{x_N = 0\}$ for example, a negative value of the product of $x_N(t_i) \cdot x_N(t_{i+1})$ and a negative value of $x_N(t_i)$ at the same time can indicate a one-sided intersection of the trajectory with Σ. Then the fine time step $\Delta\tau$ represents the distance in t direction from t_i to the intersecting point of the line connecting $(t_i, x_N(t_i))$ and $(t_{i+1}, x_N(t_{i+1}))$ with t coordinate in (t, x_N) plane:

$$\Delta\tau = \frac{|x_N(t_i)|t_{i+1} + x_N(t_{i+1})t_i}{|x_N(t_i)| + x_N(t_{i+1})}. \tag{6}$$

(ii) In each processing sequence, the cell $\mathbf{z}^j = (Z_1, Z_2, \ldots, Z_{N-1})$ is also recorded as function of j by $N-1$ one-dimensional temporary arrays $\{C_i(j) = Z_i, \quad i = 1, 2, \ldots, N-1\}$. When assigning global properties to all cells in the processing sequence before termination, there is no need to integrate the system from the initial conditions again, contrary to SCM, but just read from $\{C_i(j)\}$ to obtain the cells. Even in dealing with a new periodic motion, the period of the motion can also be found by checking the coordinates from the last cell backward until they meet again.

(iii) Generally, d_1 should be set quite small to determine a steady state motion in a numerical integration to assure a periodic motion to be found accurately. This means that a cell can be met many times before the present sequence is terminated and its character is determined. The cell can either be the component of the newly found periodic orbit or be the domain of attraction of the orbit but not its component. Comparatively, a transient motion approaching to an existing periodic motion can be found much earlier. So d_2 can be much larger than d_1.

(iv) A trajectory may leave and return into the region $\mathbf{S}$ several times before being attracted to a periodic motion. When the mapping points are outside $\mathbf{S}$, the sequence number j is still increasing but $C_i(j)$ is recorded as a fixed number, for example $Z_{i\max} + 1$, in case $1 \leqslant Z_i \leqslant Z_{i\max}$, $i = 1, 2, \ldots, N-1$. This ensures that (a) the character of a new periodic motion can still be correctly determined when part of its intersection points in steady state are outside $\mathbf{S}$; and (b) the determined properties can be assigned to all cells inside $\mathbf{S}$.

2.3. Remarks

We define the proposed process as "mapping trajectory pursuit"(MTP) because the actual positions of mapped points on Σ represent the cells which are followed through, even when leaving the domain of interest $\mathbf{S}$ until the final determination. Comparing with other existing cell mapping-based methods, the main advantages of the proposed approach can be summarized below.

(i) In the MTP process, the size of $\mathbf{S}$ can be set much smaller than that in the other methods, because it is unnecessary to contain the entire steady state orbits of the systems in the R^N state space, but only all or part of their intersecting points on Σ. In contrast, the cell size can be reasonably larger because the criterion applied in the numerical integration procedures is used to determine whether a newly mapped point is the representing point of the cell. So, the larger cell size would not produce much error in the determination of the periodic solutions. These two aspects mean that the amount of the required cells in the calculation can be reduced substantially. Note that such a reduction is based on the application of the spatial Poincaré sections. This makes the proposed approach favorable for the global study of high-order dynamical systems.

Indeed, computer memory is needed for the $N-1$ $(N-1)$-dimensional arrays $\boldsymbol{R}(\mathbf{z})$ to record the coordinates of $\mathbf{x}$. Supposing the amount of cells is $\bar{N}$, there are totally $(N-1)\bar{N}$ elements included in $\boldsymbol{R}(\mathbf{z})$. But comparing with the great reduction in the amount of cells, the introduction of the extra $(N-1)\bar{N}$ elements is tolerable.

(ii) Due to the reduction in the amount of cells, the computer time can be reduced considerably. More time is needed to cope with a new periodic motion due to the application of "exact" solution. It is only a little portion of the whole procedure in the global analysis. On the other hand, the time increase can be compensated by the introduction of $\{C_i\}$ by which the time spent in the property assignments is greatly shortened.

(iii) In SCM and ICM procedures, a large amount of data is required to be manipulated because they display the detailed information of the system in R^N state space. But in the proposed method, one deals only with the intersecting points on the Poincaré section requiring fewer amounts of data. MTP pays little attention to the detailed information of the system; hence it is appropriate for the determination of the stability boundary as a function of the initial conditions, or domains of attraction. It is also easier to distinguish two periodic motions on the $(N-1)$-dimensional Poincaré section than that on the N-dimensional state space when their orbits are near to each other.

In determining the stability boundary as a function of the initial conditions, the whole process can end if the properties of all points in **Q** are determined even when some cells inside **S** have not been dealt with.

3. Analysis of a nonlinear aeroelastic system

Consider a rigid wing of constant chord pivoted at its root in bending and torsion when there is no stiffness coupling between the motions, Fig. 2. The equations of motion of the two-degree-of-freedom aeroelastic system are described (Hancock et al., 1985) as

$$\mathbf{A}\ddot{q} + (\rho V\mathbf{B} + \mathbf{D})\dot{q} + (\rho V^2\mathbf{C} + \mathbf{E})q = 0, \tag{7}$$

where $q = (\gamma, \theta)^{\mathrm{T}}$, γ is the bending angle (+ve wing tip down), θ the torsional angle (+ve nose up), ρ the air density, and V the air (or the wing) speed. The matrices **A**, **B**, **D**, **C** and **E** are the mass, aerodynamic damping, structural damping, aerodynamic stiffness and structural stiffness matrices, respectively, which are

$$\mathbf{A} = \begin{bmatrix} I_\gamma & I_{\gamma\theta} \\ I_{\gamma\theta} & I_\theta \end{bmatrix}, \quad \mathbf{B} = \begin{bmatrix} \frac{cs^3a}{6} & 0 \\ -\frac{c^2s^2ea}{4} & -\frac{c^3s}{2}M_{\dot\theta} \end{bmatrix}, \quad \mathbf{C} = \begin{bmatrix} 0 & \frac{cs^2a}{4} \\ 0 & -\frac{c^2sea}{2} \end{bmatrix}, \quad \mathbf{E} = \begin{bmatrix} k_\gamma & 0 \\ 0 & \frac{k_{BL}(\theta)}{\theta} \end{bmatrix},$$

where I_γ, I_θ and $I_{\gamma\theta}$ are the moments of inertia in bending, in pitching and the corresponding product of inertia, respectively; k_γ is the bending stiffness. The parameters c, s, e and a are the chord length, the wing semi-span, the nondimensional distance of flexural axis from aerodynamic center and the two-dimensional sectional lift curve slope, respectively. Eqs. (7) are derived using quasi-steady aerodynamics with the addition of the nondimensional aerodynamic torsional damping derivative $M_{\dot\theta}$ representing the main unsteady aerodynamics effect. For simplicity, the structural damping **D** is ignored. This approximation is not serious here as we are using the system as a tool to demonstrate the use of the proposed cell mapping method.

In this paper, k_{BL} is a bilinear stiffness in torsional direction such that, in Fig. 3,

$$k_{BL}(\theta) = \begin{cases} K'_\theta\theta & |\theta| < g, \\ gK'_\theta + (\theta - g)K_\theta & \theta > g, \\ -gK'_\theta + (\theta + g)K_\theta & \theta < -g. \end{cases} \tag{8}$$

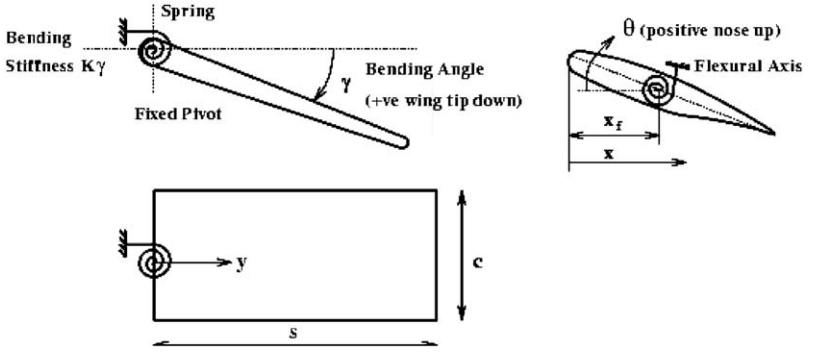

Fig. 2. Schematic of the rectangular wing model.

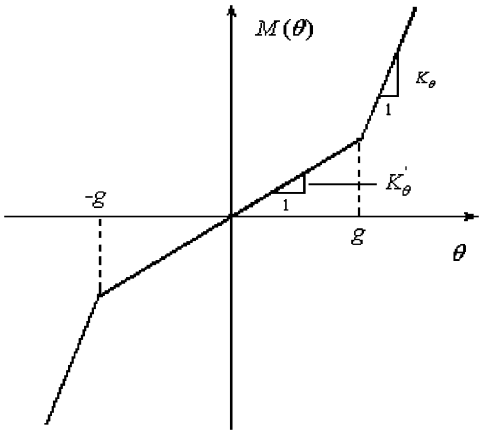

Fig. 3. Bilinear stiffness in the torsional direction.

Introducing the dimensionless variables

$$\bar{t} = \omega_\theta t, \quad \bar{\gamma} = \frac{\gamma}{g}, \quad \bar{\theta} = \frac{\theta}{g}, \quad \bar{q} = (\bar{\gamma}, \bar{\theta})^{\mathrm{T}}$$

and the dimensionless matrices $\bar{\mathbf{A}}$, $\bar{\mathbf{B}}$, $\bar{\mathbf{C}}$ and $\bar{\mathbf{E}}$,

$$\bar{\mathbf{A}} = \begin{bmatrix} 1 & \dfrac{I_{\gamma\theta}}{I_\gamma} \\ \dfrac{I_{\gamma\theta}}{I_\theta} & 1 \end{bmatrix}, \quad \bar{\mathbf{B}} = \begin{bmatrix} \dfrac{cs^3 a}{6I_\gamma} & 0 \\ -\dfrac{c^2 s^2 ea}{4\omega_\theta I_\theta} & -\dfrac{c^3 s M_{\dot{\theta}}}{2\omega_\theta I_\theta} \end{bmatrix}, \quad \bar{\mathbf{C}} = \begin{bmatrix} 0 & \dfrac{cs^2 a}{4\omega_\theta^2 I_\gamma} \\ 0 & -\dfrac{c^2 sea}{2\omega_\theta^2 I_\theta} \end{bmatrix}, \quad \bar{\mathbf{E}} = \begin{bmatrix} \left(\dfrac{\omega_\gamma}{\omega_\theta}\right)^2 & 0 \\ 0 & \dfrac{\bar{k}_{BL}(\bar{\theta})}{\bar{\theta}} \end{bmatrix},$$

where $\omega_\theta = \sqrt{K_\theta / I_\theta}$, $\omega_\gamma = \sqrt{K_\gamma / I_\gamma}$, and $\bar{k}_{BL}(\bar{\theta})$ is the dimensionless bilinear stiffness defined by

$$\bar{k}_{BL}(\bar{\theta}) = \begin{cases} k\bar{\theta} & |\bar{\theta}| < 1 \\ \bar{\theta} + k - 1 & \bar{\theta} > 1 \\ \bar{\theta} - k + 1 & \bar{\theta} < -1 \end{cases}, \quad \left(k = \frac{K'_\theta}{K_\theta}\right), \tag{9}$$

one gets the dimensionless equation of motion of the system in the form of Eq. (6) with $\mathbf{D} = 0$ after dropping all overbars for convenience.

In the following analysis, we take the system parameters as

$$s = 10\,\mathrm{m}, \quad c = 3\,\mathrm{m}, \quad a = 2\pi, \quad m = 200\,\mathrm{kg}, \quad e = 0.25, \quad \rho = 1.225\,\mathrm{kg/m^3}, \quad M_{\dot{\theta}} = -0.1,$$

$$x_{cm} = 0.6c, \quad y_{cm} = 0.6s, \quad x_f = 0.5c, \quad I_\gamma = \frac{ms^2}{3}, \quad I_\theta = mc^{4/3} x_{cm}^{2/3} + m(x_{cm} - x_f)^2,$$

$$I_{\gamma\theta} = m(x_{cm} - x_f)0.45s, \quad k_\gamma = (4\pi)^2 I_\gamma, \quad k_\theta = (20\pi)^2 mc^2/12,$$

where m is the mass of the wing, (x_{cm}, y_{cm}) the coordinates of center of mass, and x_f the distance of flexural axis from the wing leading edge, respectively.

3.1. The equilibrium position

The equilibrium positions of system (7) are obtained by setting all time derivative terms to zero

$$(\rho V^2 \mathbf{C} + \mathbf{E})q = 0. \tag{10}$$

Due to the characteristics of bilinear stiffness, the system has two kinds of equilibrium positions:

(i) trivial equilibrium position: taking $k_{BL}(\theta) = k\theta$ ($|\theta| < 1$) and solving Eq. (10) results in $q = 0$ ($\gamma = \theta = 0$);

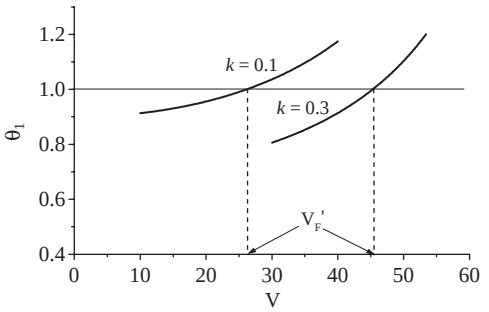

Fig. 4. The relationship between the nontrivial equilibrium position and the speed of wing, for $k = 0.1$: $V'_F = 26.2\,\mathrm{m/s}$; $k = 0.3$: $V'_F = 45.3\,\mathrm{m/s}$.

(ii) nontrivial equilibrium positions: taking $k_{BL}(\theta) = \theta + k - 1$ $(\theta > 1)$ or $k_{BL}(\theta) = \theta - k + 1$ $(\theta < 1)$, one gets the solutions of (10), (γ_1, θ_1) and (γ_2, θ_2), respectively, as

$$\begin{cases} \gamma_{1,2} = \mp \dfrac{\rho c s^2 a (1-k) V^2}{4K_\gamma \left(1 - \dfrac{\rho c^2 sea}{2K_\theta} V^2\right)}, \\ \theta_{1,2} = \pm \dfrac{1-k}{1 - \dfrac{\rho c^2 sea}{2K_\theta} V^2}. \end{cases} \tag{11}$$

The relationships of θ_1 with the wing speed V for $k = 0.1$ and 0.3 are shown in Fig. 4. The curves intersect with line $\theta_1 = 1$ at V'_F. Obviously, Eq. (10) is effective only when $V > V'_F$.

3.2. Flutter analysis

Letting $k_{BL}(\theta) = k\theta$, we rewrite Eq. (7) as

$$\begin{bmatrix} \dot{\gamma} \\ \ddot{\gamma} \\ \dot{\theta} \\ \ddot{\theta} \end{bmatrix} = \begin{bmatrix} 0 & 1 & 0 & 0 \\ a_1 & a_2 & a_3 & a_4 \\ 0 & 0 & 0 & 1 \\ b_1 & b_2 & b_3 & b_4 \end{bmatrix} \begin{bmatrix} \gamma \\ \dot{\gamma} \\ \theta \\ \dot{\theta} \end{bmatrix}, \tag{12}$$

where

$$a_1 = -\frac{h_\theta k_\gamma}{\omega_\theta^2}, \quad a_2 = -\frac{\rho a c s}{12\omega_\theta}(3ces h_{\gamma\theta} + 2s^2 h_\theta)V,$$

$$a_3 = k h_{\gamma\theta} I_\theta - \frac{\rho a c s}{4\omega_\theta^2}(s h_\theta + 2ce h_{\gamma\theta})V^2, \quad a_4 = -\frac{\rho s c^3 M_{\dot{\theta}}}{2\omega_\theta} h_{\gamma\theta} V,$$

$$b_1 = \frac{h_{\gamma\theta} k_\gamma}{\omega_\theta^2}, \quad b_2 = \frac{\rho a c s}{12\omega_\theta}(3ces h_\gamma + 2s^2 h_{\gamma\theta})V,$$

$$b_3 = -k h_\gamma I_\theta + \frac{\rho a c s}{4\omega_\theta^2}(s h_{\gamma\theta} + 2ce h_\gamma)V^2, \quad b_4 = \frac{\rho s c^3 M_{\dot{\theta}}}{2\omega_\theta} h_\gamma V,$$

in which

$$h_\gamma = \frac{I_\gamma}{I_\gamma I_\theta - I_{\gamma\theta}^2}, \quad h_\theta = \frac{I_\theta}{I_\gamma I_\theta - I_{\gamma\theta}^2}, \quad h_{\gamma\theta} = \frac{I_{\gamma\theta}}{I_\gamma I_\theta - I_{\gamma\theta}^2}.$$

The eigenvalues of the coefficient matrix of Eq. (12) satisfy the following characteristic equation:

$$\lambda^4 + \beta_1 \lambda^3 + \beta_2 \lambda^2 + \beta_3 \lambda + \beta_4 = 0, \tag{13}$$

where $\beta_1 = -(a_2 + a_4)$, $\beta_2 = a_2 b_4 - a_4 b_2 - a_1 - b_3$, $\beta_3 = a_1 b_4 + a_2 b_3 - a_3 b_2 - a_4 b_1$, $\beta_4 = a_1 b_3 - a_3 b_1$. According to Routh's criteria, when the following conditions are satisfied (on condition that $\beta_1 > 0$ which is definitely true for

system (7)):

$$\beta_1\beta_2\beta_3 - \beta_1^2\beta_4 - \beta_3^2 = 0. \tag{14}$$

The flutter motion (limit cycle oscillation or LCO) with nondimensional frequency

$$\omega_F = \sqrt{\frac{\beta_3}{\beta_1}}, \tag{15}$$

will be generated from the trivial equilibrium position $q = 0$ when $V > V_F$, where V_F is the solution of Eq. (14) and defined as the flutter speed. The relationships of V_F and ω_F with the ratio $k = K'_\theta/K_\theta$ are shown in Fig. 5. Calculations reveal that there is no real solution V_F from Eq. (13) in case $k < k_L \approx 0.38$. So, the trivial equilibrium position of Eq. (7) is locally stable and no flutter will be excited under disturbances. But after a critical value V_{LT} is exceeded for the wing speed V, LCOs can still be excited from the trivial equilibrium position under larger disturbances. The relationship of V_{LT} with k is also roughly depicted in Fig. 5, which looks like the continuation of V_F. This problem will also be considered later using the proposed CM method. The LCOs, one for the system with $k = 0.5$, $V > V_F = 12.2\,\mathrm{m/s}$ and under small initial condition (T_2), and another for $k = 0.1$, $V > V_{LT} \approx 10\,\mathrm{m/s}$ and under a rather larger initial condition (T_1), respectively, are shown in Fig. 6. Obviously, the LCOs in the two cases are symmetrical to the trivial equilibrium position $q = 0$.

As mentioned above, there are two nontrivial equilibrium positions, (γ_1, θ_1) and (γ_2, θ_2) when $V \geqslant V'_F$. In fact, their existence implies instability of the trivial equilibrium position, $q = 0$ if the local stability of the trivial equilibrium state continued until V overpasses V'_F under small disturbances. So, the relationship of V'_F and k has actual meaning only for $k < k_L$, as shown in Fig. 5. When the dimensionless displacement in the θ direction is increased to greater than 1, the

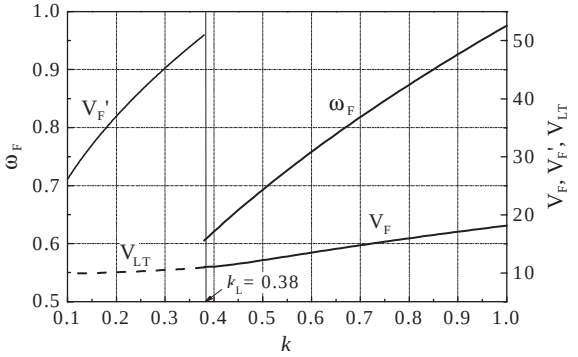

Fig. 5. The flutter frequency ω_F and the critical speed V_F (the trivial equilibrium position calculated by Eq. (13)), V_{LT} (the trivial equilibrium position under larger initial conditions) and V'_F (the nontrivial equilibrium positions calculated by Eq. (11)).

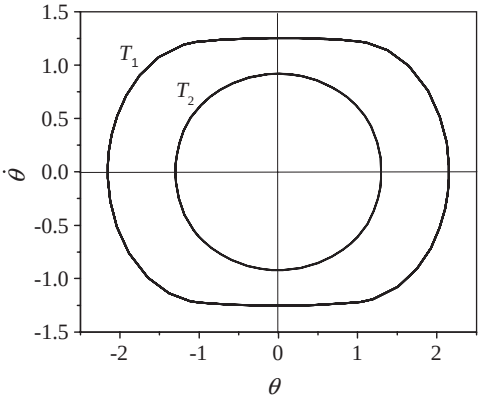

Fig. 6. The symmetrical LCOs around the trivial equilibrium position for T_1: $k = 0.1$, $V = 10\,\mathrm{m/s}$, $\Gamma_0 = (0, 0, 2, 0)$ and T_2: $k = 0.5$, $V = 13\,\mathrm{m/s}$, $\Gamma_0 = (0, 0, 0.1, 0)$. $\Gamma_0 = (\gamma(0), \dot{\gamma}(0), \theta(0), \dot{\theta}(0))$ is the initial condition).

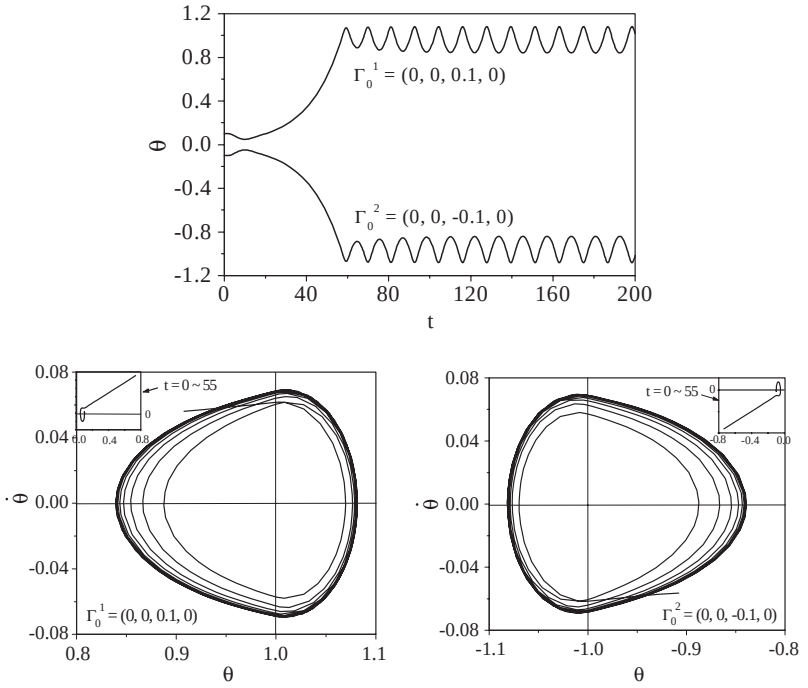

Fig. 7. The asymmetrical LCOs around the nontrivial equilibrium positions, for $k = 0.1$, $V = 30\,\mathrm{m/s}$.

divergent motion starting off from $q = 0$ can be suppressed because the stiffness of the system for $|\theta| \geqslant 1$ is larger than that for $|\theta| < 1 (K_\theta > K'_\theta)$. So the steady state motion of the system will form a LCO around one of the nontrivial equilibrium positions, but unsymmetrical in the θ direction because of the different values of K_θ from K'_θ, as shown in Fig. 7.

4. Application of the improved CM method for flutter analysis

As mentioned in Section 2, the hyperplane Σ should be located at a zero value of the velocity coordinate to cope with the stable equilibrium points and limit cycles. In the following analysis, we take $\dot{\theta} = 0$ as Σ and take the one-sided intersections when the trajectory passes through Σ from negative $\dot{\theta}$ to positive $\dot{\theta}$ as the point-to-point maps (3). The cell sizes are determined by $h_1 = 0.05$, $h_2 = 0.02$ and $h_3 = 0.05 \sim 0.1$ in the γ, $\dot{\gamma}$ and θ direction, respectively. The domain of interest $\mathbf{S}$ on Σ should be chosen to cover at least part of, if not all, the intersecting points of the steady state trajectory on Σ. The range of $\mathbf{S}$ over γ is $(-1.5, 1.5)$ and over $\dot{\gamma}$ is $(-0.6, 0.6)$. In the θ direction, the range can be adjusted to let the amount of the cells to be as small as possible. Letting $\bar{d} = \left[\left(h_1^2 + h_2^2 + h_3^2\right)/2\right]^{1/2}$, we take $d_1 = 0.01 \sim 0.03\bar{d}$ and $d_2 = 0.1 \sim 0.3\bar{d}$. For simplicity, the initial condition region $\mathbf{Q}$ includes only the initial conditions in the θ direction, and we always have $\gamma(0) = 0$, $\dot{\gamma}(0) = 0$.

4.1. Determination of domains of attraction

In case $k < k_L$, the trivial equilibrium position of the system is locally stable for $V < V'_F$, so the motion is damped under small disturbances as initial conditions. But LCOs can be excited by larger disturbances when $V > V_{LT}$. Letting $k = 0.1$, the domains of attraction are determined using the proposed CM method as in Figs. 8 and 9, which show the different motions as functions of $V \sim \theta(0)$, $V \sim \dot{\theta}(0)$ and $\theta(0) \sim \dot{\theta}(0)$. The motions are classified as: damped stable motion to the trivial equilibrium position, limit cycle oscillation (LCO), complicated periodic motion with period n ($n \geqslant 2$), chaotic motion, and divergent flutter. Referring to the θ coordinate, the LCOs are either symmetric centered at $\theta = 0$ or asymmetric centered at $\theta = +1$ or $\theta = -1$. Though the proposed method is mainly appropriate for dealing

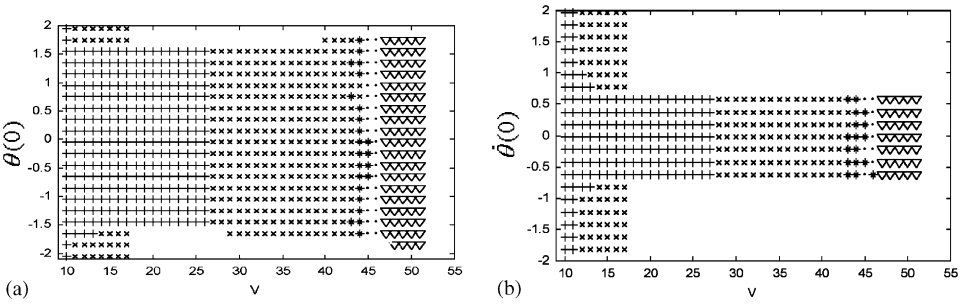

Fig. 8. Domains of attraction: (a) torsion angle versus wing speed ($\gamma(0)=\dot{\gamma}(0)=\dot{\theta}(0)=0$); (b) torsion velocity versus wing speed ($\gamma(0)=\dot{\gamma}(0)=\theta(0)=0$). $+$, damped stable motion; $\times$, LCO; $*$, period 2 motion; $\bullet$, periodic motion with period greater than 2; ∇, chaotic motion; blank, divergent motion.

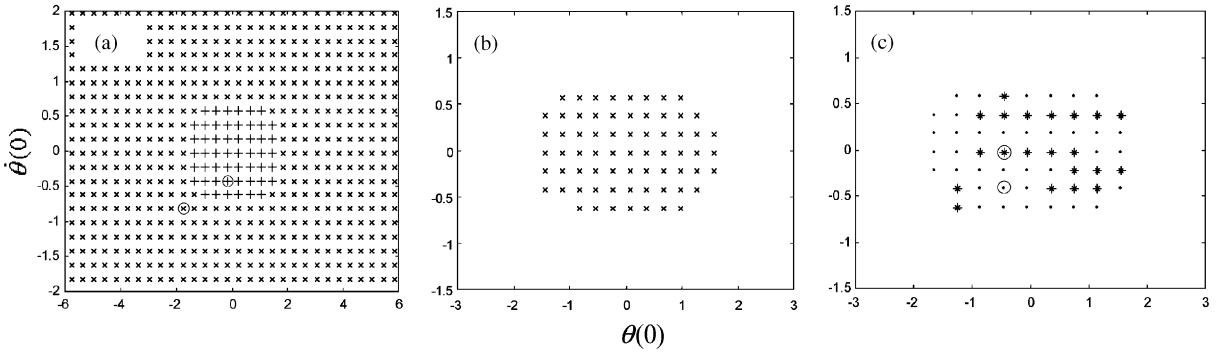

Fig. 9. Domains of attraction for torsion velocity versus torsion angle ($k=0.1$) for: (a) $V=15\,\mathrm{m/s}$; (b) $V=30\,\mathrm{m/s}$; (c) $V=45\,\mathrm{m/s}$.

with periodic motions with limited periods, it can still be used to determine a chaotic motion by taking it as a periodic one with a relatively long period, for example, longer than 100, or by finding a nondivergent motion without periodicity after 200 iterates on Σ. For the aeroelastic problem in this paper, chaotic motions at one or another fixed wing speed were found with period over a range from 100 to 200 on the spatial Poincaré. The results were also confirmed by the exact numerical integration and FFT analysis. The Lyapunov exponent is not reliable because of the nonsmooth nature of the bilinearity as mentioned in Price et al. (1994).

In Fig. 8, the domains of attraction in the planes $(V,\theta(0))$ and $(V,\dot{\theta}(0))$ are displayed over a broad range of the airspeed V. The **Q**s are one-dimensional spaces defined in the θ and $\dot{\theta}$ direction, respectively. Fixing wing speed V, the initial values are taken from **Q**s successively from the lowest value to the highest one with certain intervals. Small initial conditions, say $|\theta(0)|<1.5$ or $|\dot{\theta}(0)|<0.6$, result in damped motions to the trivial equilibrium position for $V<V_F'=26.2\,\mathrm{m/s}$, asymmetrical LCOs over the velocity range $26.2<V<43\,\mathrm{m/s}$, and complicated periodic motions with period $\geqslant 2$ and chaotic motion over the approximate velocity range $43<V<52\,\mathrm{m/s}$. The divergent flutter happens at $V\approx 52\,\mathrm{m/s}$. For large initial conditions, $|\theta(0)|>1.5$ or $|\dot{\theta}(0)|>0.6$, symmetrical LCOs occur when $V>V_{LT}\approx 10\,\mathrm{m/s}$ (see the boundary line $V_{LT}\sim k$ in Fig. 5). However, the motion becomes divergent under larger disturbances for $V\geqslant 18\,\mathrm{m/s}$.

Similar to Fig. 8, the domains of attraction in the two-dimensional plane $(\theta(0),\dot{\theta}(0))$ are shown in Fig. 9 for V equal to 15, 30 and 45 m/s, respectively. In the three cases, the domains of interest **S** in the θ direction were set to be $(-4.5, 4.5)$, $(-1.3, 1.3)$ and $(-3, 3)$, while the cell sizes are 0.1, 0.05 and 0.1, respectively. Note that in the first two cases, the size of **Q** in the θ direction is larger than that of $\mathbf{S}(\theta\cap\mathbf{S})$. To prove the results in Fig. 8 and 9, the phase portraits of the torsional motion for $V=15$ and 45 m/s are shown in Fig. 10. The points with circles ($\oplus$, $\otimes$, $\circledast$, $\odot$) in Fig. 9 are selected as initial values to display different steady motions successively: (a) damped stable motion; (b) symmetrical LCO; (c) periodic motion with period 2; and (d) periodic motion of period 7. To display the steady state orbits clearly, the transient motions are omitted in (c) and (d).

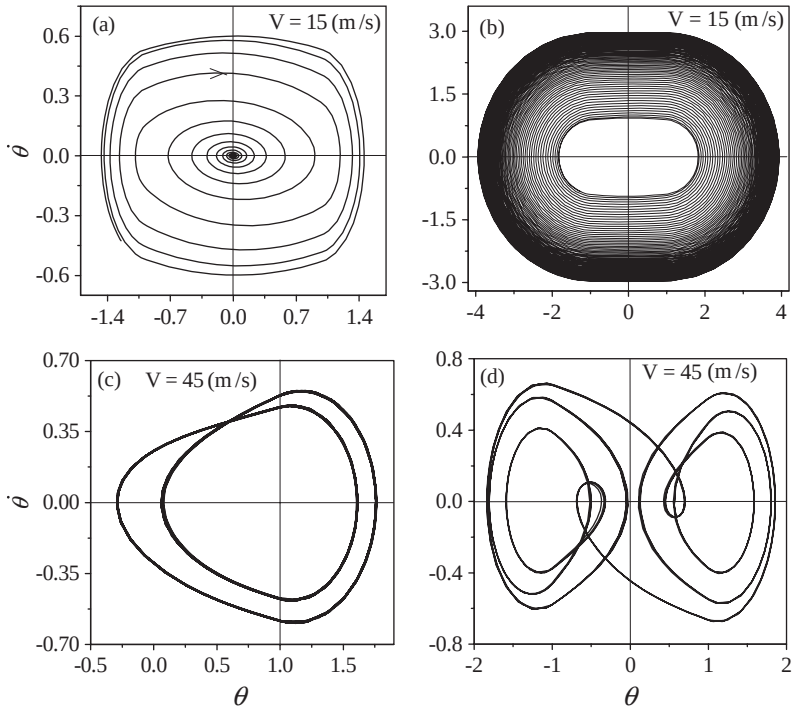

Fig. 10. Phase portraits for: (a) $\Gamma_0 = (0, 0, -0.25, -0.425)$; (b) $\Gamma_0 = (0, 0, -1.45, -0.825)$; (c) $\Gamma_0 = (0, 0, -0.45, 0)$; (d) $\Gamma_0 = (0, 0, -0.45, -0.425)$.

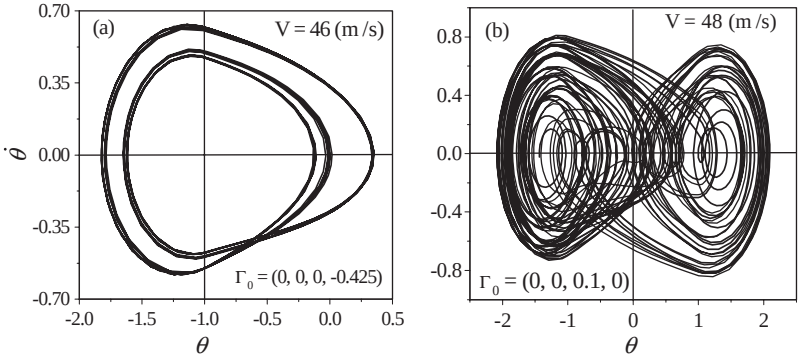

Fig. 11. Phase portraits $(\theta, \dot{\theta})$ for: (a) period-3 motion; (b) chaotic motion.

From Fig. 8, we know that chaotic motion happens when the wing speed V is between 47–51 m/s under some initial conditions. Before the occurrence of chaotic motion, the motion at $V = 46\,\mathrm{m/s}$ seems to be of period 3, but also with some quasiperiodic character, as shown in Fig. 11.

4.2. The bifurcation diagrams

Bifurcation diagrams are an important tool for characterizing the dynamics of nonlinear systems over a broad range of the system parameters. Two algorithms are often used to calculate the bifurcation diagrams: the brute-force algorithm and the continuation method (Parker and Chua, 1989). Calculation of the Frechet derivative is needed in using the continuation method. So, the method cannot be used for the nonsmooth dynamical system like that of Eq. (7). The brute-force algorithm is simple and can tackle the problem in a straightforward manner. But because it is hard to

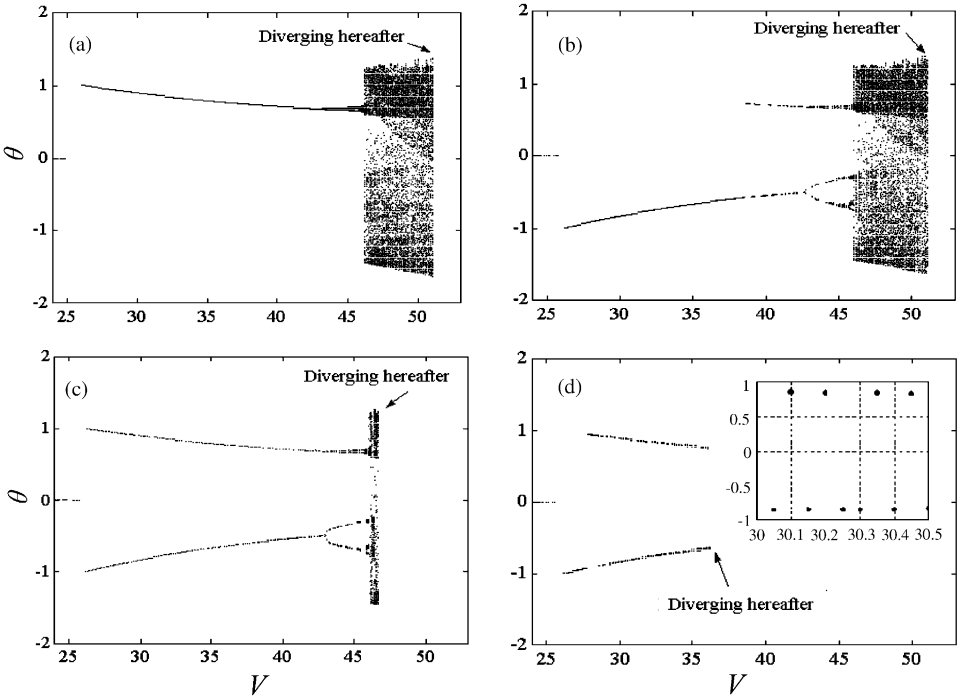

Fig. 12. The bifurcation diagrams of torsional angle ($k = 0.1$) for: (a) $\Delta\dot{\theta} = 0$; (b) $\Delta\dot{\theta} = -0.1$; (c) $\Delta\dot{\theta} = -0.3$; (d) $\Delta\dot{\theta} = -0.5$.

predict whether the steady state solutions have been achieved, the number of iterations of the simulation should be set large enough for all control parameter values over the mentioned range. So the brute-force algorithm is often time-consuming and inefficient. In addition, the enhancement by using the Newton–Raphson techniques to find steady state solutions cannot be applied for nonsmooth dynamical systems. However, the proposed CM method can be used to obtain bifurcation diagrams efficiently, because steady state motion can be recognized immediately. The bifurcation diagrams for the torsional displacement as a function of the wing velocity V are calculated and shown in Fig. 12. Generally, to reduce the duration of the transient, the final condition in the steady state of the kth simulation is used as the initial condition for the $(k+1)$th simulation in simulating a Poincaré map over the control parameter range. Because we are interested in the effect of disturbances on the aeroelastic behavior of the system over a broad range of wing speed, a small disturbance $\Delta\dot{\theta}$ was added to the final value of $\dot{\theta}$ at each velocity, and $(\dot{\theta} + \Delta\dot{\theta})$ was taken as the initial condition in the $\dot{\theta}$ direction for determining the response in the next augmented velocity. The adding of $\Delta\dot{\theta}$ represents an abrupt disturbance to the aeroelastic system, which brings an instantaneous velocity change in the θ direction; $\Delta\dot{\theta}$ is equal to 0, –0.1, –0.3 and –0.5, respectively, in Fig. 12.

Fig. 12(a) shows that asymmetrical LCOs exist over the velocity range $26.2 < V < 43$ m/s, before entering the chaotic regime. In that velocity range, the centers of the LCOs remain unchanged. But when small disturbances, say $\Delta\dot{\theta} = -0.1$, are added, the LCOs change their centers from $\theta = -1$ to $\theta = +1$, or vice versa, as the velocity exceeds 38 m/s approximately. As the level of disturbance is increased, the changes of the LCO centers happen at lower and lower velocities. The changes are shown clearly in Fig. 12(d) over the velocity range $30 < V < 30.5$ m/s. Large disturbances, say $\Delta\dot{\theta} = -0.5$, can even cause diverging of the motion before the chaotic regime is entered, as shown in Fig. 12(d).

4.3. Comparisons

Because of the introduction of the MTP procedure, the domains of attraction of the system can always be correctly determined, no matter whether the transient trajectory leaves **S** temporarily or not during simulations. Such an advantage is especially important when integrations start off from points outside of **S**, because the size of the initial condition analysis region **Q** can be set different from that of the domain of interest **S.** Otherwise, some points inside but near the border of the domain of attraction of a specific kind of motion could be wrongly determined. For example, using a Poincaré-like simple cell mapping (PLSCM) method without trajectory pursuit process for $V = 15$ and 30 m/s ($k = 0.1$), respectively, would result in the domains of LCOs as shown in Fig. 13. One finds that the size of the domains

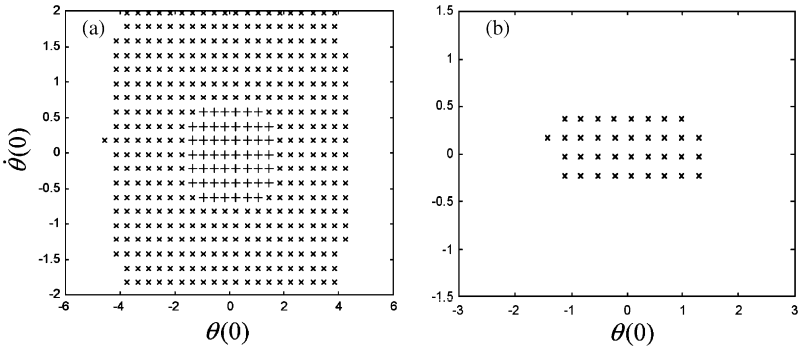

Fig. 13. Domains of attraction for torsion velocity versus torsion angle obtained by use of the PLSCM method without trajectory pursuing process ($k = 0.1$) for: (a) $V = 15\,\mathrm{m/s}$; (b) $V = 30\,\mathrm{m/s}$.

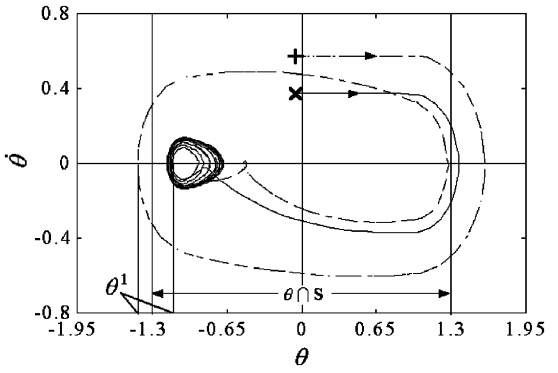

Fig. 14. The trajectory starting off from the initial point "+" was determined as a divergent one in Fig. 13(b) because the first mapping point on Σ is out of the **S**.

of LCOs in Fig. 13 is smaller than those in Fig. 9. Some points were wrongly determined to be divergent (sink cells), since the trajectory starting off from them intersect with Σ (resulting in mapping points) but outside **S**, as shown in Fig. 14.

The proposed CM method results in further reduction of the memory requirements and in improvement of the accuracy of the calculations, comparing to that of the PLSCM and PLICM methods. On the other hand, it is obvious that the computer resources needed for the Poincaré-type cell techniques, such as the PLSCM, PLICM and the proposed CM method, are much smaller than those required by the SCM and ICM methods. To illustrate the efficiency of the proposed CM method, direct numerical integrations of Eq. (7) were carried out to yield domains of attraction for $V = 15$ and $45\,\mathrm{m/s}$ ($k = 0.1$). As expected, the results obtained by direct numerical integration are the same to what presented in Figs. 9(a) and (c). All calculations in this paper were performed on a PC with Pentium III CPU at 733 MHz, and by use of the computing software MATLAB. The function ODE23S was found suitable for integration of Eqs. (7). In obtaining the domain of attraction shown by Fig. 9(a) using the direct numerical integration, the number of 150 cycles of phase trajectory was found to be an adequate duration to achieve a steady state periodic solution from each initial condition. But only the output data among the last 20 cycles were recorded and used to determine the limit cycle to which the initial point is attracted. For most initial points, calculation over 150 cycles of phase trajectory is obviously too long to acquire the steady state solutions. Take $\dot{\theta}(0) = -2.45$ and $\dot{\theta}(0) = -0.425$ for example; 24.88 CPU seconds were required to complete the calculation. But in fact it needed only 6.65 CPU seconds approximately to achieve the periodic solution. To obtain Fig. 9(a), the direct numerical integration required 211 CPU minutes. Using the proposed CM method, only 14 CPU minutes was required; i.e., the proposed method is 15 times faster than the direct numerical integration.

In obtaining the domain of attraction shown in Fig. 9(c) using the direct numerical integration, the number of 90 cycles of phase trajectory was found to be adequate to achieve a periodic solution (of period 2, 3 or 7) from each initial condition, except the "sink cells". For the latter case, the simulation stopped as soon as $\dot{\theta}$ was found greater than 15 and

the initial point was then believed to be of a "sink". Calculations showed that usually only 5–7 cycles were needed to satisfy the "stop" condition when starting off the calculation from a "sink" initial point. As a result, constructing Fig. 9(c) requires only 8.2 CPU minutes using the direct numerical integration. In consideration of using 3.7 CPU minutes, the proposed CM method is still faster, though only 2.2 times in this case.

5. Conclusion

By introducing the "mapping trajectory pursuit" (MTP) technique to the cell mapping method on spatial Poincaré sections, both the amount of cells and the computational time can be greatly reduced. The global dynamic properties of all cells in analysis sequences can accurately be determined. The definition of the initial condition analysis region makes the method especially appropriate for predicting the stability boundary as a function of initial conditions (or domains of attraction).

Using the improved method, a binary aeroelastic system with bilinear structural nonlinearity in the θ direction was investigated. Different types of motions dependent of initial conditions, including damped stable motion, limit cycle oscillation (LCO), complicated periodic motion, chaotic motion and divergent flutter, were determined for the aeroelastic system with a certain degree of bilinear structural nonlinearity. The results agreed well with the stability analysis. The bifurcation diagrams obtained by the proposed method show that under the influence of disturbances in the torsional direction, the center of LCOs jumps between the positive and negative equilibrium points, as the wing speed is increased. Larger disturbances cause the motion to diverge at rather low wing speeds. In comparison with the direct numerical integration, the proposed CM method appears to be efficient in revealing the global behaviour of high order nonlinear dynamical systems.

Acknowledgements

This research was supported by the NNSF of PR China under Grant #10272078 and an SRG grant #7001664 of City University of Hong Kong. The authors also thank Professor Païdoussis for linguistically processing the manuscript.

References

Chen, J.S., Chian, C.H., 2001. Effects of crank length on the dynamics behavior of a flexible connecting rod. ASME Journal of Vibration and Acoustics 123, 318–323.

Hancock, G.J., Wright, J.R., Simpson, S., 1985. On the teaching of the principles of wing flexure-torsion flutter. Aeronautical Journal 89, 285–305.

He, Q., Xu, W., Rong, H.W., Fang, T., 2004. Stochastic bifurcation in Duffing–van der Pol oscillators. Physica A-Statistical Mechanics and its Applications 338, 319–334.

Hsu, C.S., 1980. A theory of cell-to-cell mapping dynamical system. Journal of Applied Mechanics 47, 931–939.

Hsu, C.S., 1981. A generalized theory of cell-to-cell mapping for nonlinear dynamical system. Journal of Applied Mechanics 48, 634–642.

Hsu, C.S., 1982. A probabilistic theory of nonlinear dynamical systems based on the cell state concept. Journal of Applied Mechanics 49, 895–902.

Hsu, C.S., 1987. Cell-to-cell mapping: a method of global analysis for nonlinear systems. Springer, New York.

Hsu, C.S., Guttalu, R.S., 1980. An unravelling algorithm for global analysis of dynamical systems: an application of cell-to-cell mappings. Journal of Applied Mechanics 47, 940–948.

Karlberg, M., Aidanpaa, J.O., 2003. Numerical investigation of an unbalanced rotor system with bearing clearance. Chaos, Solitons and Fractions 18, 653–664.

Kim, S.H., Lee, I., 1996. Aeroelastic analysis of a flexible airfoil with a freeplay non-linearity. Journal of Sound and Vibration 193, 823–846.

Levitas, J., Weller, T., 1995. Poincaré linear interpolated cell mapping: method for global analysis of oscillating system. Journal of Applied Mechanics 62, 489–495.

Levitas, J., Weller, T., Singer, J., 1994. Poincaré-like simple cell mapping for non-linear dynamical system. Journal of Sound and Vibration 176, 641–662.

Librescu, L., Chiocchia, G., 2003. Implications of cubic physical/aerodynamic non-linearities on the character of the flutter instability boundary. International Journal of Non-Linear Mechanics 38, 173–199.

Mu, M., Duan, W.S., Chou, J.F., 2004. Recent advances in predictability studies in China (1999–2002). Advances in Atmospheric Sciences 21, 437–443.

Parker, T.S., Chua, L.O., 1989. Practical Numerical Algorithms for Chaotic Systems. Springer, New York.
Price, S.J., Lee, B.H.K., Alighanbari, H., 1994. An analysis of the post-instability behaviour of a two-dimensional airfoil with a structural nonlinearity. Journal of Aircraft 31, 1395–1401.
Raghothama, A., Narayanan, S., 2002. Periodic response and chaos in nonlinear systems with parametric excitation and time delay. Nonlinear Dynamics 27, 341–365.
Singh, S.N., Brenner, M., 2003. Limit cycle oscillation and orbital stability in aeroelastic systems with torsional nonlinearity. Nonlinear Dynamics 31, 435–450.
Tang, D., Conner, M.D., Dowell, E.H., 1998. Reduced-order aerodynamic model and its application to a nonlinear aeroelastic system. Journal of Aircraft 35, 332–338.
Tongue, B.H., Gu, K., 1988. Interpolated cell mapping of dynamical systems. Journal of Applied Mechanics 55, 461–466.
Yang, Z.C., Zhao, L.C., 1990. Analysis of limit cycle flutter of an airfoil in incompressible flow. Journal of Sound and Vibration 123, 1–13.
Zhao, L.C., Yang, Z.C., 1990. Chaotic motions of an airfoil with nonlinear stiffness in incompressible flow. Journal of Sound and Vibration 138, 245–254.
Zufiria, P.J., Martinez-Marin, T., 2003. Improved optimal control methods based upon the adjoining cell mapping technique. Journal of Optimization Theory and Applications 118, 657–680.